

INCLUSIVE LOW Q^2 MEASUREMENTS AT HERA

V. LENDERMANN

*Kirchhoff-Institut für Physik, Universität Heidelberg
Im Neuenheimer Feld 227, 69120 Heidelberg Germany
E-mail: victor@kip.uni-heidelberg.de*

Inclusive ep scattering measurements at low virtualities of the exchanged boson, Q^2 , allow precision tests of perturbative QCD at high gluon densities, as well as studies of the transition from the perturbative to non-perturbative QCD domain. Measurements in the transition region require special experimental approaches due to the limited detector acceptance. The current status and results of low Q^2 measurements at HERA are summarised.

1. Introduction

Inclusive measurements of ep scattering are the main source for our knowledge of proton structure. Over several decades, they have played a decisive role in the development of Quantum Chromodynamics (QCD). So far the greatest kinematic coverage, over five magnitudes in the Bjorken scale variable x and in the modulus of the four-momentum transfer squared Q^2 , is reached by the H1 and ZEUS experiments at HERA. Their inclusive DIS data^{1,2,3,4,5} have shown that the Q^2 evolution of the proton structure function $F_2(x, Q^2)$ is well described by perturbative QCD (pQCD) in the range of $Q^2 \gtrsim 2 - 3 \text{ GeV}^2$. The data reach 2 – 3% precision for Q^2 values up to $\sim 100 \text{ GeV}^2$.

At $Q^2 \lesssim 2 - 3 \text{ GeV}^2$ the transition takes place into a domain in which non-perturbative effects dominate and the assumption of asymptotic freedom is no longer valid. A proper treatment of the transition from soft to hard QCD regime can thus improve our understanding of quark confinement. The description of the transition region remains a challenge for the theory and a field for phenomenological models.

The recent measurements performed at $Q^2 \lesssim 2 - 3 \text{ GeV}^2$ are presented in the following section. Afterwards, studies of the F_2 behaviour and comparisons to models are discussed. In the last section, extractions of the longitudinal structure function F_L are described.

2. Measurements in the Transition Region

The acceptance of main H1 and ZEUS detectors is limited to $Q^2 \gtrsim 2 \text{ GeV}^2$, therefore special experimental techniques are necessary to access the transition region. One way is to use special low Q^2 devices⁷ mounted close to the outgoing lepton beam direction. However, the region $0.8 \lesssim Q^2 \lesssim 2 \text{ GeV}^2$ is not reached via these devices since the respective angular range of the scattered lepton is complicated by the instrumentation of the main calorimeters.

This region is covered by data collected in special runs with the interaction vertex shifted in the direction of the proton beam^{8,9,10}. In such an experimental configuration the scattered lepton is detected at higher polar angles^a in the main detector, thus gathering events at lower Q^2 values.

In Fig. 1 the reduced cross section

$$\sigma_r = \frac{Q^4 x}{2\pi\alpha^2} \frac{d^2\sigma}{dx dQ^2} = F_2(x, Q^2) - \frac{y^2}{Y_+} F_L(x, Q^2), \quad (1)$$

with the inelasticity $y = Q^2/(xs)$ and $Y_+ = 1 + (1-y)^2$, is shown. The ZEUS Beam Pipe Tracker (BPT) measurements⁷, the preliminary H1 results of running in 1999 with the standard vertex position and in 2000 with the vertex shifted by 70 cm¹⁰ are shown together with the fixed target data from NMC¹¹. The HERA inclusive data in the transition domain reach 3 – 4% precision. The predictions of the extrapolated Fractal model fit¹² and the ALLM97 parametrisation¹³ are also displayed. All predictions are in good agreement with the data.

The low Q^2 measurements are further extended towards higher x values making use of events with hard photon radiation. The cross section for radiative processes becomes sufficiently large for distinct experimental configurations, in which the photon is emitted either nearly collinear with the electron beam (Initial State Radiation, ISR) or nearly collinear with the scattered lepton (Final State Radiation, FSR), or both the lepton and the photon are detected under finite polar angles nearly back-to-back in azimuth (QED Compton process, QEDC). Two of these topologies, ISR and QEDC, are used for measurements, as discussed below.

2.1. Cross Section Measurement Using ISR Data

The new H1 ISR analysis uses the shifted vertex data collected in 2000. Contrary to the previous HERA measurements^{14,15,16}, the emitted photon

^aThe polar angle is measured w.r.t. the proton beam direction. A higher polar angle means a lower scattering angle for the outgoing lepton.

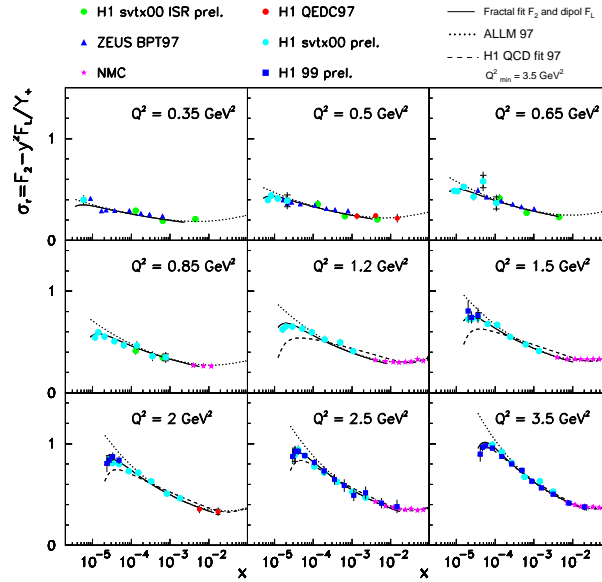


Figure 1. Reduced cross section measurements at $Q^2 \lesssim 3 \text{ GeV}^2$ by H1 (preliminary), ZEUS and NMC compared with the ALLM97 parametrisation and with a calculation based on the fractal fit to F_2 and F_L from the dipole model.

is not tagged explicitly in the new H1 ISR analysis¹⁷. Instead, its energy is inferred from the longitudinal momentum imbalance:

$$2E_\gamma = 2E_e^0 - (E - p_z)_e - (E - p_z)_h, \quad (2)$$

where E_e^0 is the electron beam energy, $(E - p_z)_e$ is the measured difference between the energy and the longitudinal momentum of the scattered electron and $(E - p_z)_h$ is the same quantity for the hadronic final state. As in the other recent H1 low Q^2 measurements, the Backward Silicon Tracker (BST) is used to identify the scattered electron and to reduce the contamination by neutral particle backgrounds.

The new data cover the region $0.35 \lesssim Q^2 \lesssim 0.85 \text{ GeV}^2$ and $10^{-4} \lesssim x \lesssim 5 \cdot 10^{-3}$. They are in a good agreement with the other measurements, as shown in Fig. 1.

2.2. F_2 Measurement Using QED Compton Scattering

The experimental signature of QEDC events is an approximately back-to-back azimuthal configuration of the outgoing electron and photon, both

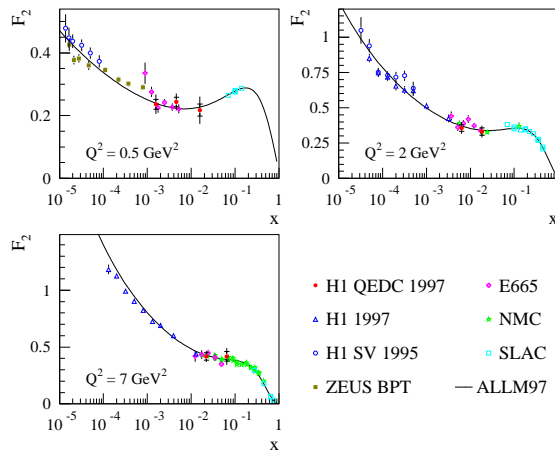


Figure 2.
 F_2 measurements from QED Compton scattering by H1 (closed circles), compared with other measurements at HERA and fixed target experiments. The solid line depicts the ALLM97 parametrisation.

found in the main detector. In this configuration their transverse momenta nearly balance such that it is possible to reconstruct the event kinematics for very small values of Q^2 .

The first F_2 measurement in inelastic QEDC scattering is performed by H1¹⁸ using data from the 1997 running period. A prominent background to inelastic QEDC scattering arises from inclusive DIS events in which one particle from the hadronic final state (typically a π^0) fakes the outgoing photon. At high y , where the hadronic final state lies mostly in the backward region, this process dominates the QEDC signature, hampering a clean QEDC event selection. For this reason the measurement is restricted to relatively low y values: $y \lesssim 0.006$.

At so low y the variables x and y cannot be determined solely from the measured electron and photon four-momenta, since their resolution deteriorates as $1/y$. Hence for the kinematic reconstruction the Σ -method is employed, which also uses information from the hadronic final state. As low y values correspond to small polar angles of the final state hadrons, one of the main challenges for the analysis is the correct reconstruction of the total momentum of the hadronic final state accounting for losses beyond the forward acceptance of the detector. This necessitates a good simulation of hadronisation processes at low Q^2 and low invariant masses of the hadronic final state W . The simulation of the hadronic final state down to the resonance region is performed using the SOPHIA program¹⁹.

The F_2 values measured in QED Compton scattering are shown in Fig. 2 as a function of x at fixed Q^2 and are compared with other HERA^{1,7,8} and fixed target^{11,20,21} data. The QEDC analysis extends the kinematic range

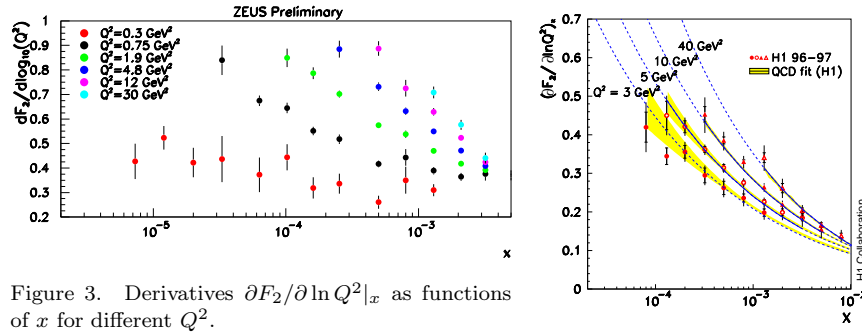


Figure 3. Derivatives $\partial F_2/\partial \ln Q^2|_x$ as functions of x for different Q^2 .

of HERA at low Q^2 towards higher x values, thus complementing standard inclusive and shifted vertex measurements. The measurement is consistent with the results of fixed target experiments in the overlapping region. The data are well described by the ALLM97 parametrisation¹³.

3. Interpretation of the Data

A principal feature of the HERA data is the dramatic rise of F_2 at low x driven by the gluon evolution. This rise questions the validity of the DGLAP⁶ approach, on which the current pQCD fits to the data are based, in the region of high parton densities. While in the DGLAP formalism only the $\ln Q^2$ terms are summed, the subleading terms involving powers of $\alpha_s \ln(1/x)$ may become large as x decreases. This may require a different summation scheme, such as BFKL²² or CCFM²³, or non-linear corrections to the pQCD expansion²⁴. The non-linear effects may lead to gluon-gluon absorption which would tame the growth of F_2 at low x .

High precision F_2 data at very low x are necessary in order to search for deviations from the DGLAP evolution and signs of saturation. As low x can only be reached at low Q^2 due to kinematical correlation, it is the low Q^2 data which are used for these studies.

An important quantity for searches of a new gluon dynamics is the derivative $\partial F_2(x, Q^2)/\partial \ln Q^2|_x$ describing scaling violations. The local derivatives measured by H1¹ and ZEUS are shown in Fig. 3 as functions of x for different Q^2 . They exhibit a continuous rise towards low x down to the lowest Q^2 without an indication of a change in the dynamics. The derivatives are well described by the pQCD calculations for $Q^2 \gtrsim 3 \text{ GeV}^2$.

In the double asymptotic limit, the DGLAP evolution equation can be solved analytically and F_2 is expected to rise approximately as a power of x towards low x . A power behaviour is also predicted in BFKL. A

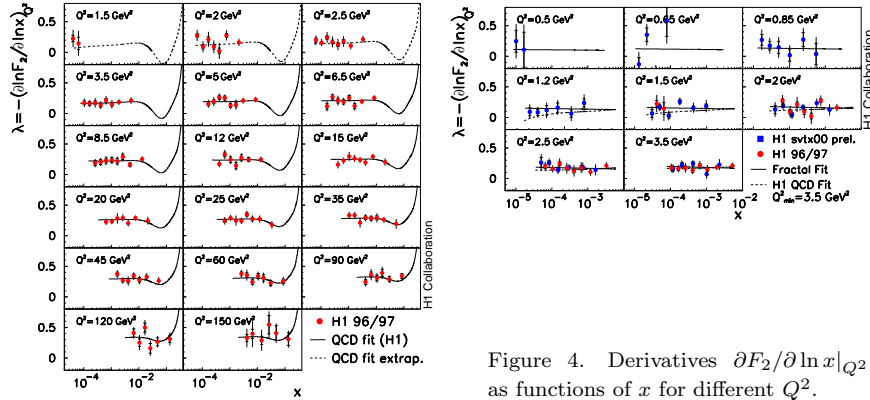


Figure 4. Derivatives $\partial F_2 / \partial \ln x|_{Q^2}$ as functions of x for different Q^2 .

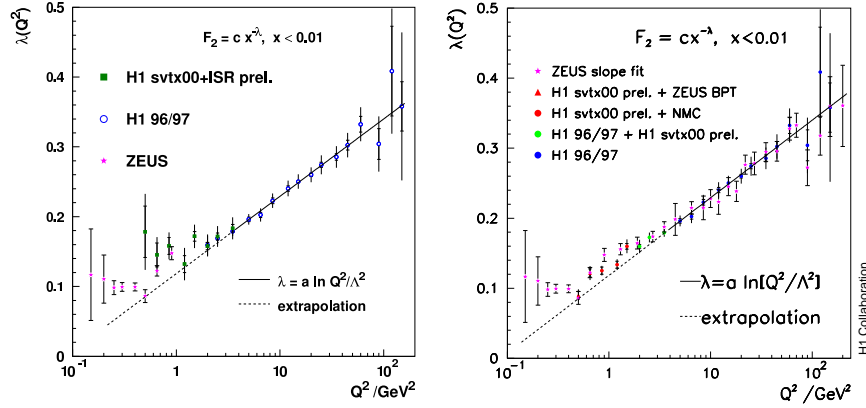
damping of this rise would indicate the presence of novel QCD effects. A relevant observable for the investigation of the dynamics of this growth is the derivative $\lambda = -\partial F_2(x, Q^2) / \partial \ln x|_{Q^2}$.

The high precision of the present F_2 data allowed H1 to measure this quantity locally^{10,25}, as shown in Fig. 4. The measurements are consistent with no dependence of λ on x for $x < 0.01$. The monotonic rise of F_2 persists down to the lowest x measured at HERA, and no evidence for a change of this behaviour is found.

This suggests that F_2 can be parameterised by $F_2 = c(Q^2) \cdot x^{-\lambda(Q^2)}$. The results, obtained by fitting the present data at fixed Q^2 values are shown in Fig. 5. The left plot presents $\lambda(Q^2)$ values obtained separately from the H1 and ZEUS data. The extension of the x range of the H1 shifted vertex data achieved by including the ISR data allowed an improved extraction of λ . The highest precision can probably be reached by combining H1, ZEUS and fixed target data, as shown in the right plot.

The coefficient $c(Q^2) \approx 0.18$ and the logarithmic dependence of λ on Q^2 for $Q^2 \gtrsim 2 - 3 \text{ GeV}^2$ are in accord with pQCD predictions. In contrast, at lower Q^2 the behaviour is changing to a weaker dependence compatible with reaching, as $Q^2 \rightarrow 0$, a constant consistent with the soft pomeron intercept $\alpha_P - 1 = 0.08$ which is expected from the energy dependence of soft hadronic interactions²⁸. The change takes place at distance scales of $\sim 0.3 \text{ fm}$ and can be interpreted as being related to a transition from partonic to hadronic degrees of freedom. This change is the major challenge for the theory which must interpolate between the two x dependences.

For many approaches, colour dipoles appear to provide useful degrees of freedom in order to treat low x inclusive and diffractive data²⁹. Among

Figure 5. Selected HERA results of the λ extraction from low x data.

several dipole models, the saturation model³⁰ has been a subject of much debate. Using just a few parameters, the model successfully describes the transition region at low x via the saturation of the colour dipole–proton cross section at large transverse sizes of the dipole. The extended model³¹ includes the gluon DGLAP evolution in order to describe the scaling violations in the perturbative region (see Fig. 6 left).

The saturation model predicts a geometric scaling of the γ^*p cross section in the small x region³². This means that the cross section σ_{γ^*p} should be a function of only one dimensionless variable $\tau = Q^2 R_0^2(x)$ where the “saturation radius” $R_0(x)$ decreases with decreasing x . The HERA and fixed target data at $x < 0.01$ exhibit this behaviour, as shown in Fig. 6 right. This scaling is a manifestation of the presence of an internal saturation scale, $Q_s(x) \sim 1/R_0(x)$, characterising dense partonic systems.

However, despite the success of the saturation model and its appeal from the theoretical point of view, there is no compelling evidence for the saturation at low x yet, as other models are also able to describe the data with a similar precision.

4. Extraction of F_L

The proton structure function F_L describes the exchange of longitudinally polarised photons. It imposes a constraint on the otherwise highly uncertain behaviour of the gluon distribution function in the proton at low Q^2 . Though the gluon density is obtained in pQCD analyses of DIS data via the derivative $\partial F_2/\partial Q^2$, its determination at low Q^2 and low x suffers from

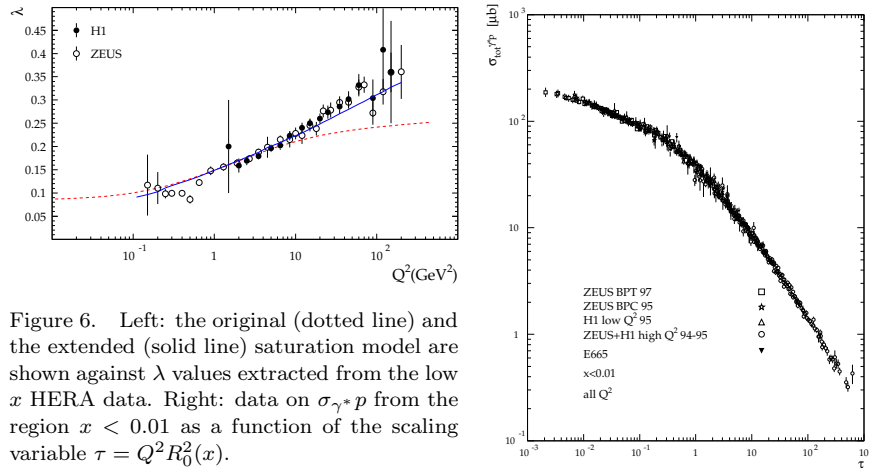


Figure 6. Left: the original (dotted line) and the extended (solid line) saturation model are shown against λ values extracted from the low x HERA data. Right: data on σ_{γ^*p} from the region $x < 0.01$ as a function of the scaling variable $\tau = Q^2 R_0^2(x)$.

non-perturbative effects becoming significant.

A direct determination of F_L needs cross section values measured at different y values for the same x and Q^2 . This can be achieved at lower ep centre-of-mass energies, e.g. by performing dedicated runs at lower proton beam energies. The possibility of taking such runs at the end of the HERAII running period is currently being discussed³³.

Alternatively, events with tagged Initial State Radiation can be employed, as presented by ZEUS¹⁶. The ISR process is interpreted as the inclusive ep scattering at a reduced electron beam energy. The emitted photon is detected in the luminosity monitor. The result of the ZEUS analysis of the data taken during 1996 and 1997 running periods are shown in Fig. 7. Much more statistics is required in order to achieve a sufficient accuracy of the F_L measurement in ISR.

A higher accuracy is achieved using indirect methods of F_L extraction, which are based on the analysis of the reduced cross section behaviour at high y values. The data of the minimum bias 1999²⁶ and shifted vertex 2000¹⁰ runs are used by H1²⁷ to extract F_L by two methods: the “derivative method” and the new “shape method”.

In the derivative method, F_L is extracted from the partial derivative of the cross section on y at fixed Q^2

$$\left. \frac{\partial \sigma_r}{\partial \ln y} \right|_{Q^2} \approx \left. \frac{\partial F_2}{\partial \ln y} \right|_{Q^2} - \frac{2y^2(2-y)}{Y_+^2} F_L \quad (3)$$

which is dominated by the F_L -dependent term at high y .

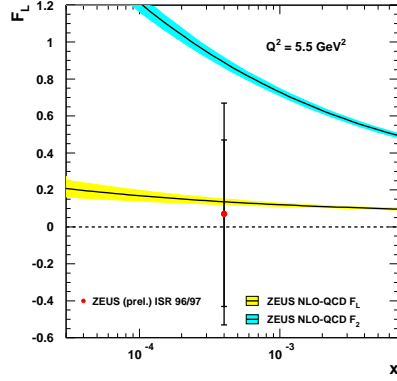


Figure 7. ZEUS ISR result for F_L plotted for $x = 4 \cdot 10^{-4}$ and $Q^2 = 5.5 \text{ GeV}^2$. The yellow band shows the prediction for F_L from the ZEUS NLO QCD fit³. The light blue band shows the prediction for F_2 , which is the maximum possible value of F_L .

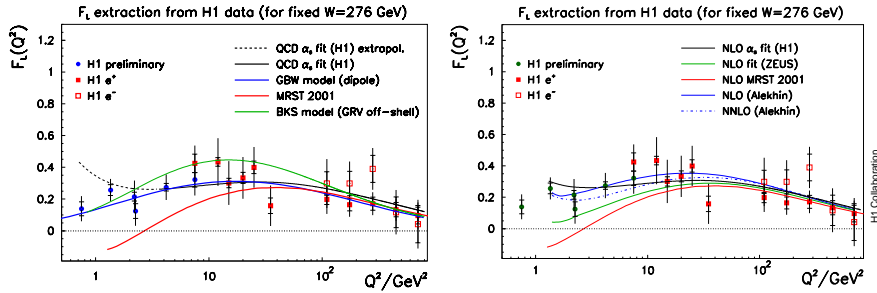


Figure 8. Q^2 dependence of $F_L(x, Q^2)$ at fixed $y = 0.75$, extracted from the H1 data. The lines represent various phenomenological models, as well as pQCD fits.

The shape method exploits the shape of σ_r in a given Q^2 bin. The shape is driven at high y by the kinematic factor y^2/Y_+ (eq. 1), and to a lesser extent by $F_L(x, Q^2)$ which is considered to be constant: $F_L = F_L(Q^2)$. Based on the analysis of the rise of F_2 towards low x , the reduced cross section is fitted by

$$\sigma_{r,\text{fit}} = cx^{-\lambda} - \frac{y^2}{Y_+} F_L, \quad (4)$$

and F_L is determined from the fit for different Q^2 bins. The errors obtained turn out to be significantly smaller than those from the derivative method. However, the x -dependence cannot be extracted.

The results for a fixed $y = 0.75$ ($W = 276 \text{ GeV}$), are presented in Fig. 8, in which an overview of all current H1 data in the Q^2 range $0.75 \leq Q^2 \leq 700 \text{ GeV}^2$ is given. The data are compared with higher order QCD fits. The H1 data favour a positive, not small F_L at low Q^2 .

References

1. C. Adloff *et al.* [H1 Collaboration], *Eur. Phys. J. C* **21**, 33 (2001).
2. S. Chekanov *et al.* [ZEUS Collaboration], *Eur. Phys. J. C* **21**, 443 (2001).
3. S. Chekanov *et al.* [ZEUS Collaboration], *Phys. Rev. D* **67**, 012007 (2003).
4. C. Adloff *et al.* [H1 Collaboration], *Eur. Phys. J. C* **30**, 1 (2003).
5. S. Chekanov *et al.* [ZEUS Collaboration], *Phys. Rev. D* **70**, 052001 (2004).
6. V. N. Gribov and L. N. Lipatov, *Sov. J. Nucl. Phys.* **15**, 438 and 675 (1972);
L. N. Lipatov, *Sov. J. Nucl. Phys.* **20**, 94 (1975);
Y. L. Dokshitzer, *Sov. JETP* **46**, 641 (1977);
G. Altarelli and G. Parisi, *Nucl. Phys. B* **126**, 298 (1977).
7. J. Breitweg *et al.* [ZEUS Collaboration], *Phys. Lett. B* **487**, 53 (2000).
8. C. Adloff *et al.* [H1 Collaboration], *Nucl. Phys. B* **497**, 3 (1997).
9. M. Derrick *et al.* [ZEUS Collaboration], *Z. Phys. C* **69**, 607 (1996).
10. H1 Collaboration, Contributed paper to EPS 2003, Aachen, Abstract **082**.
11. M. Arneodo *et al.* [New Muon Collaboration], *Nucl. Phys. B* **483**, 3 (1997).
12. T. Laštovička, *Eur. Phys. J. C* **24**, 529 (2002).
13. H. Abramowicz and A. Levy, DESY-97-251, hep-ph/9712415.
14. T. Ahmed *et al.* [H1 Collaboration], *Z. Phys. C* **66**, 529 (1995).
15. M. Derrick *et al.* [ZEUS Collaboration], *Z. Phys. C* **69**, 607 (1996).
16. ZEUS Collaboration, Contributed paper to EPS 2003, Aachen, Abstract **502**.
17. H1 Collaboration, Contrib. paper to ICHEP 2004, Beijing, Abstract **5-0170**.
18. A. Aktas *et al.* [H1 Collaboration], *Phys. Lett. B* **598**, 159 (2004).
19. A. Mücke *et al.*, *Comput. Phys. Commun.* **124**, 290 (2000).
20. L. W. Whitlow *et al.*, *Phys. Lett. B* **282**, 475 (1992).
21. M. R. Adams *et al.* [E665 Collaboration], *Phys. Rev. D* **54**, 3006 (1996).
22. E. A. Kuraev, L. N. Lipatov and V. S. Fadin, *Sov. JETP* **44**, 443 (1976);
E. A. Kuraev, L. N. Lipatov and V. S. Fadin, *Sov. JETP* **45**, 199 (1977);
I. I. Balitsky and L. N. Lipatov, *Sov. J. Nucl. Phys.* **28**, 822 (1978).
23. M. Ciafaloni, *Nucl. Phys. B* **296**, 49 (1988);
S. Catani, F. Fiorani and G. Marchesini, *Phys. Lett. B* **234**, 339 (1990);
S. Catani, F. Fiorani and G. Marchesini, *Nucl. Phys. B* **336**, 18 (1990);
G. Marchesini, *Nucl. Phys. B* **445**, 49 (1995).
24. L. V. Gribov, E. M. Levin and G. M. Ryskin, *Phys. Rept.* **100**, 1 (1983);
A. H. Mueller and J. Qiu, *Nucl. Phys. B* **268**, 427 (1986).
25. C. Adloff *et al.* [H1 Collaboration], *Phys. Lett. B* **520**, 183 (2001).
26. H1 Collaboration, Contributed paper to EPS 2001, Budapest, Abstract **799**.
27. H1 Collaboration, Contrib. paper to ICHEP 2004, Beijing, Abstract **5-0161**.
28. A. Donnachie and P. V. Landshoff, *Phys. Lett. B*, **296**, 227 (1992);
A. Donnachie and P. V. Landshoff, *Z. Phys. C*, **61**, 139 (1994).
29. G. Shaw, these proceedings.
30. K. Golec-Biernat and M. Wüsthoff, *Phys. Rev. D* **59**, 014017 (1999);
K. Golec-Biernat and M. Wüsthoff, *Phys. Rev. D* **60**, 114023 (1999).
31. J. Bartels, K. Golec-Biernat, H. Kowalski, *Phys. Rev. D* **66**, 014001 (2002).
32. A. M. Stasto, K. Golec-Biernat, J. Kwiecinski, *Phys. Rev. Lett.* **86**, 596 (2001).
33. J. Feltesse, these proceedings; R. Thorne, these proceedings.